**RESEARCH ARTICLE**

# Assessment of strength and leaching characteristics of heavy metal–contaminated soils solidified/stabilized by cement/fly ash

Fusheng Zha[1] · Chunjie Ji[1] · Long Xu[1] · Bo Kang[1] · Chengbin Yang[1] · Chengfu Chu[1]

## Abstract

Solidification/stabilization technique has been widely adopted to remediate the heavy metal–contaminated sites. In the present work, the strength and leaching characteristics of the contaminated soils solidified/stabilized by cement/fly ash were systemically investigated. Electrical resistivity was also measured to establish empirical relationships for assessment of remediation efficacy. Tests results showed that the unconfined compressive strength increased and the leached ion concentration decreased with increasing curing time. In contrast, the unconfined compressive strength decreased and the leached ion concentration increased with increasing initial heavy metal ion concentration in the specimen. For the strength characteristic, the most notable detrimental effect was induced by $Cr^{3+}$ and the least was induced by $Pb^{2+}$. For the leaching characteristic, the trend was reversed. The electrical resistivity of the tested specimen increased significantly with increasing curing time and with decreasing initial ion concentration. The electrical resistivity of the Pb-contaminated specimen was higher than that of the Zn-contaminated specimen, which in turn was higher than that of the Cr-contaminated specimen. Empirical relationships between the strength, leaching characteristic, and electrical resistivity were established, which could be adopted to assess the remediation efficacy of heavy metal–contaminated soil solidified/stabilized by cement/fly ash.

## Introduction

Widespread contamination of soils by heavy metals is one of the most severe environmental problems because it can seriously deteriorate the quality of the environment and human health. Many kinds of remediation techniques have been

**Highlights**
• Strength, leaching, and electrical characteristics of the contaminated soils solidified/stabilized by cement/fly ash are explored.
• Remediation efficiency of soils contaminated by Pb, Zn, and Cr are investigated and compared.
• Empirical relationships based on electrical resistivity are established for assessment of the remediation efficiency

Responsible editor: Zhihong Xu

✉ Long Xu
  xulong_2005@hfut.edu.cn

[1] School of Resource and Environmental Engineering, Hefei University of Technology, Hefei 230009, People's Republic of China

extensively proposed for remediation of heavy metal–contaminated sites. As a promising technique, solidification/stabilization (S/S) has been extensively adopted in engineering practices owing to its efficacy, convenience, and cost-effectiveness (Vipulanandan 1995; Suman Raj et al. 2005; Kumpiene et al. 2008; Chen et al. 2015; Liu et al. 2018).

In the S/S technique, an additive is selected and mixed with the contaminated soil to fix the harmful substances in a stable form physically or to chemically reduce their migration capacity in the soil. Investigations of additives, which include cement, lime, fly ash, alkaline residue, and bentonite, are of great importance to the remediation efficacy of the S/S technique (Spence 1992; Conner and Hoeffner 1998; Hunce et al. 2012; Chen et al. 2015; Chen et al. 2017; Li et al. 2018). Among these additives, cement has been widely adopted to solidify heavy metal–contaminated soils. Chen et al. (2010) and Zha et al. (2012) investigated the strength characteristics of cement-solidified Pb- and Zn-contaminated soils and found that the strength improved with increasing cement content and curing time. For lower initial $Pb^{2+}$

concentration, the strength of the solidified specimen increased as the $Pb^{2+}$ concentration increased, whereas the trend was reversed for specimens with higher initial $Pb^{2+}$ concentration. Moreover, a decreasing trend of the unconfined compressive strength and an increasing trend of the deformation modulus were revealed with increasing initial $Zn^{2+}$ concentration. Qiao et al. (2007) also experimentally confirmed that, for cement-solidified specimen with curing times of 28 days and 56 days, the strength decreased by 15.5% and 14.0%, respectively, due to the formation of $Pb(OH)_2$, $Cu(OH)_2$, and $Zn(OH)_2$ in the specimen. Leaching characteristic of the Cr-contaminated specimen investigated by Penilla et al. (2006) showed that the remediation efficacy of contaminated soils solidified/stabilized by cement alone was much better than that of other additives including fly ash alone and cement/fly ash mixture. In further studies, cement was partially replaced by other additives such as lime or fly ash for cost savings and eco-environmental protection. According to experiments performed by Miller et al. (2000), cement and lime could both effectively remediate As-contaminated soils to reach the environmental safety limits based on leaching and strength characteristics. Yin et al. (2006) investigated the remediation efficacy of a cement/rice husk ash mixture for Pb-contaminated soils. Test results showed that, although the unconfined compressive strength of the mixture was reduced owing to the partial replacement of cement by rice husk ash, the leaching characteristic of those soils was effectively improved compared to the soil solidified by cement alone. This was attributed to the fine particles contained in rice husk ash. Such an influence was investigated by Kumpiene et al. (2008), who observed significant decreases of $Cu^{2+}$ and $Pb^{2+}$ in contaminated soil during laboratory and in situ leaching tests when fly ash was incorporated. Yoon et al. (2002) and Cao et al. (2018) performed electrical resistivity tests on heavy metal–contaminated soils, confirming the significant effects of the initial ion concentration, curing time, and cement content on the electrical resistivity. Moreover, empirical relationships between the unconfined compressive strength and the electrical resistivity were established to assess the engineering properties of Pb-contaminated soils solidified/stabilized by cement.

Based on the balance between cost-effectiveness and strength/leaching characteristics, the adoption of cement with other additives in the S/S technique is evidently of great interest in the remediation of heavy metal–contaminated soils and is worth investigating in detail. In the present work, a series of experiments was performed to investigate the strength and leaching characteristics of Pb-, Zn-, and Cr-contaminated soils solidified/stabilized by cement/fly ash. Electrical resistivity tests were conducted as well to establish empirical relationships for assessment of remediation efficacy.

# Materials and testing methods

## Materials

The tested soils were sampled from a construction site at a depth of 4–5 m in Hefei, Anhui province, China. Following ASTM standards (ASTM D2216-10 2010 and ASTM D4318-17e1 2017), the basic physical properties of the soils, including the density, water content, specific gravity, and Atterberg limits, were determined and summarized in Table 1. The tested soil can be classified as a low liquid limit clay (CL) according to the Unified Soil Classification System (ASTM D2487-00 2000). The main mineral components of the tested soils were quartz, kaolinite, montmorillonite, and chlorite, as determined by the X-ray diffraction (XRD) technique (Fig. 1). In addition, the maximum dry density of 1.66 $g/cm^3$ and the optimal water content of 21.3% were determined by performing a proctor compaction test following the ASTM D698 - 12e2 (Fig. 2).

Cement/fly ash was adopted to remediate the contaminated soils in the present work. Ordinary Portland cement was purchased in Nanjing city, China, and fly ash was obtained from the Hefei Wanneng Power Plant. The main chemical components of the cement and fly ash were analyzed by X-ray fluorescence (XRF) technique, which are listed in Table 2. CaO, $SiO_2$, and $Al_2O_3$ were typically detected in the cement, whereas $SiO_2$, $Al_2O_3$, and $Fe_2O_3$ were mainly detected in the fly ash. The particle size distribution of the fly ash determined by using a laser particle size analyzer is shown in Fig. 3.

Pb-, Zn-, and Cr-contaminated soils were targeted for remediation in the present work owing to their typical distributions serious and hazards in China. Analytical-grade $Pb(NO_3)_2$, $Zn(NO_3)_2 \cdot 6H_2O$, and $Cr(NO_3)_3 \cdot 9H_2O$ were selected to represent the heavy metal contaminants owing to their high solubility and the low interference of the nitrate in the S/S process (Boardman 1999).

## Specimen preparation

Specimens (called C10+F30) were prepared with fixed mass ratios of cement and fly ash to dry soils of 10% and 30%, respectively, as in investigations performed by Kolias et al. (2005), Katsioti et al. (2008), and Moon et al. (2009). For comparison, contaminated specimens solidified by 10% cement (C10) or by 30% fly ash (F30) were prepared as well in the present work.

The pulverized soils and cement/fly ash powders were oven-dried at 105 °C for 24 h and sized through 2-mm and 0.5-mm sieves, respectively. Target amounts of heavy metal contaminants (with mass ratios of $Pb^{2+}$, $Zn^{2+}$, and $Cr^{3+}$ to dry soils, or concentrations equaling 0; 5,000; 10,000; and 15,000 mg/kg) were weighed and dissolved in distilled water. The solutions were mixed with the dry

**Table 1** Basic physical properties of tested soil

| Density (g/cm$^3$) | Water content (%) | Specific gravity | Liquid limit (%) | Plastic limit (%) | Plastic index | Liquidity index |
|---|---|---|---|---|---|---|
| 1.92 | 25.50 | 2.67 | 49.40 | 24.80 | 24.60 | 0.03 |

soils and cured for 3 days to obtain the contaminated soils. Next, the contaminated soil powders were oven-dried again and mixed thoroughly with the additives at the optimal water content determined as shown in Fig. 2. Finally, the prepared mixtures were put into a cylindrical mold and statically compacted to obtain specimens with a diameter of 39.1 mm, height of 80 mm, and dry density of 1.58 g/cm$^3$ (equaling 95% of the maximum dry density). The prepared specimens were cured for 0, 7, 28, or 90 days in a constant temperature and humidity curing box at a controlled temperature of 22 ± 1 °C and relative humidity of 95 ± 2%.

## Testing methods

### Unconfined compressive strength test

In accordance with the Standard Test Method for Unconfined Compressive Strength of Cohesive Soil (ASTM D2166 / D2166M-16 2016), the as-prepared specimen was assembled in the strain-controlled YHS-2 UCS testing apparatus and soaked in distilled water. The UCS test was then performed at a vertical strain rate of 1%/min. The stress and strain of the specimen were recorded at intervals of 5 s until the specimen failed.

### Toxicity characteristic leaching procedure

The leaching characteristic of the solidified contaminated specimen was determined using the toxicity characteristic leaching procedure (TCLP) following USEPA, Method 1311 1992. The prepared specimen was crushed into pieces smaller than 9.5 mm. A leachant with a pH value of 2.88 ± 0.05 was prepared by diluting 5.7 mL acetic acid (HAc) in 1 L deionized water. Next, 12.5 g of crushed specimen and 250 mL leachant (solid-to-liquid ratio of 1:20) were mixed in a polythene bottle and vibrated at a rate of 80 rpm for 18 h (Levasseur et al. 2006; Zha et al. 2018). The leachate was then filtered through a 0.45-μm filter membrane; the $Pb^{2+}$, $Zn^{2+}$, and $Cr^{3+}$ concentrations in the leachate were determined by atomic absorption spectrophotometry (AAS).

### Electrical resistivity test

The prepared specimen was statically cut into a square cylinder in 40-mm width and 20-mm height. The electrical resistivity was then measured using a GW Instek LCR-816 apparatus in accordance with the testing method elaborated in ASTM G187-05 2005. Two copper electrodes, 2 mm thick and 50 mm in diameter, were closely covered on both ends of the specimen. A frequency of 2 kHz was selected for
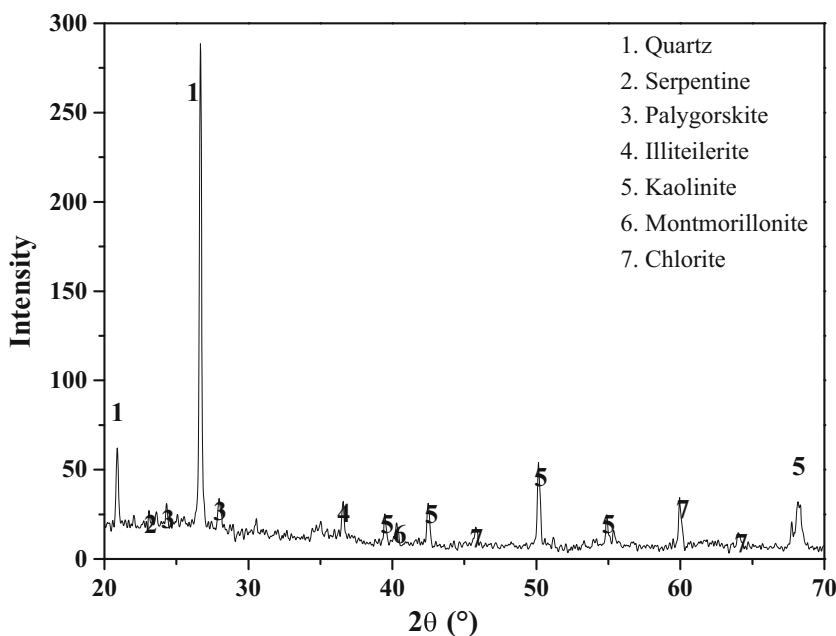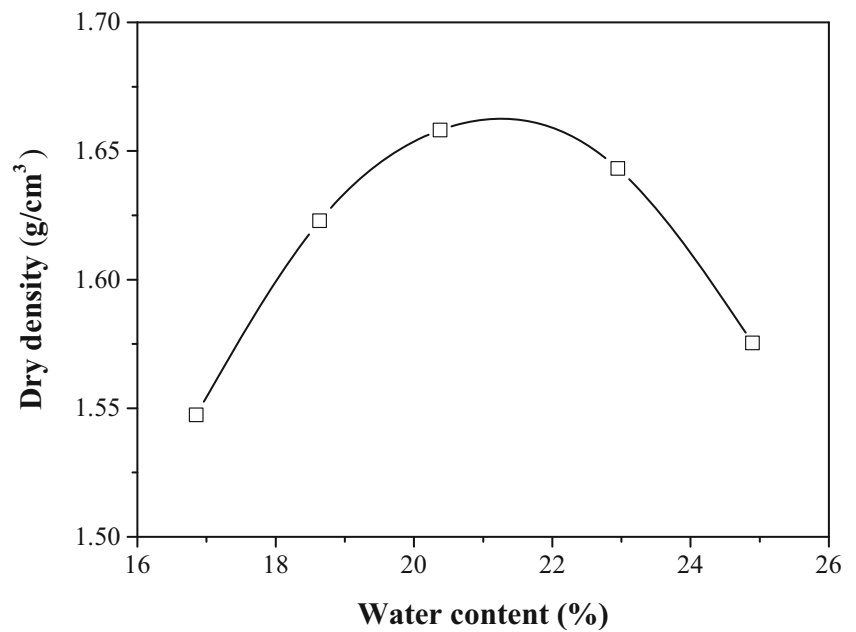
**Fig. 1** XRD results for tested soil



1. Quartz
2. Serpentine
3. Palygorskite
4. Illiteilerite
5. Kaolinite
6. Montmorillonite
7. Chlorite

**Fig. 2** Compaction curve for tested soils



measuring electrical resistivity to avoid the influence of electrode polarization and the double-layer relaxation effect (Zhang et al. 2014). The electrical resistivity test was conducted at a temperature of $20 \pm 2$ °C. A diagram of the test layout is shown in Fig. 4. Voltage and current signals were acquired simultaneously to calculate the electrical resistivity of the specimen using Eq. (1) as follows:

$$\rho = \frac{\Delta U}{I} \cdot \frac{S}{L} \qquad (1)$$

where $\rho$ (in $\Omega \cdot$m) is the electrical resistivity of the specimen; $\Delta U$ (in V) is the voltage drop applied across the specimen; $I$ (in A) is the electrical current through the specimen; $S$ (in m$^2$) is the cross-sectional area of the electrode at the two ends; and $L$ (in m) is the length of the specimen paralleled with the direction of the electrical current.

## Results and discussion

### Unconfined compressive strength

The unconfined compressive strengths as a function of curing time for the tested specimens are presented in Fig. 5.

As shown in Fig. 5, the unconfined compressive strength of the specimens with different heavy metal types and initial ion concentrations increased significantly with increasing curing time, which confirmed the remedial effects on the contaminated soils by the incorporation of cement and/or fly ash. This is because, during the S/S process, hydration reactions of the $C_2S$ ($2CaO \cdot SiO_2$), $C_3S$ ($3CaO \cdot SiO_2$), and $C_3A$ ($3CaO \cdot Al_2O_3$) mainly in the cement will result in the formation of calcium silicate hydrate gel (C-S-H) and calcium aluminate hydrate gel (C-A-H), which encapsulate the solid particles and fill the pores of the specimen. Ion exchanges between the Na$^+$ and K$^+$ on the clay particle surface and the Ca$^{2+}$ generated during cement hydration reduce the thickness of the diffusion layer and improve the strength of the specimen. Additionally, pozzolanic reactions between the redundant Ca$^{2+}$ from previous reactions and the $SiO_2$ and $Al_2O_3$ in the soil take place in an alkaline environment and generate more hydration products such as C-S-H, C-A-H, and calcium aluminum silicate hydrate (C-A-S-H) gels. These hydration reactions, ion exchanges and agglomerations, and pozzolanic reactions develop fully with increasing curing time, which consequently contribute to the improved strength, as shown in Fig. 5 (Conner and Hoeffner 1998; Kumpiene et al. 2008; Deng et al. 2015; Deng et al. 2018; Bian et al. 2018).

Results in Fig. 5 also showed that the remediation efficacy of the cement/fly ash for the contaminated specimen (C10+

**Table 2** Main chemical components of cement and fly ash

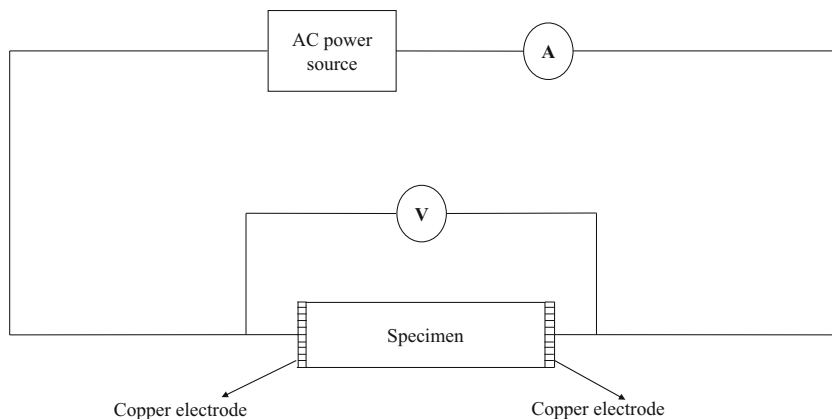| Chemical components | | CaO | SiO$_2$ | Al$_2$O$_3$ | SO$_3$ | Fe$_2$O$_3$ | MgO | TiO$_2$ | Na$_2$O |
|---|---|---|---|---|---|---|---|---|---|
| Content (%) | Cement | 43.8 | 27.2 | 9.9 | 3.0 | 2.9 | 1.6 | 0.5 | 0.4 |
| | Fly ash | 0.6 | 33.1 | 1.3 | 0.3 | 1.7 | 0.5 | 0.9 | 0.5 |

**Fig. 3** Particle size distribution of fly ash
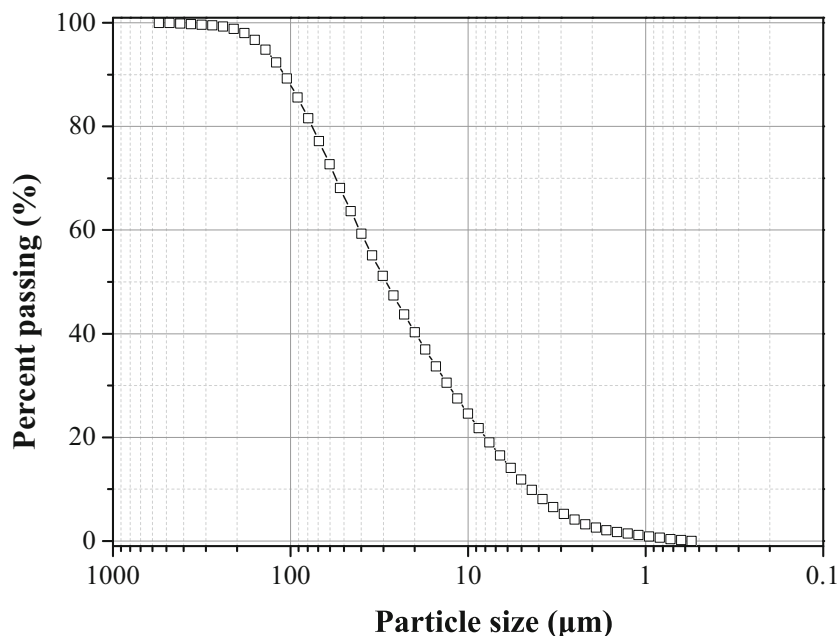


F30) was lower and higher than that of the cement (C10) and the fly ash (F30) alone, respectively, which can be attributed to the significant difference in CaO content (43.8% in cement and 0.6% in fly ash) and the alkaline environment of the cement and fly ash. However, a common conclusion would be that cement/fly ash does notably improve the strength characteristics of the specimen (Nochaiya et al. 2010; Tang et al. 2010; Liu et al. 2019).

The unconfined compressive strengths as a function of initial ion concentration for the tested specimens are presented in Fig. 6.

Results in Fig. 6 showed that the unconfined compressive strength of the cement/fly ash–solidified specimens obviously decreased with increasing initial ion concentration. Evidently, the presence of heavy metal ions, as well as the increase in initial ion concentration, results in a retardation effect on the hydration reactions, ion exchanges and agglomerations, and pozzolanic reactions of the cement/fly ash mixture (Olmo et al. 2001; Chen et al. 2007; Sophia et al. 2010; Wang et al. 2018;

Wu et al. 2018). Moreover, curves in Fig. 6 showed that the heavy metal ion type significantly influenced the strength of the specimen. The solidified specimen contaminated by Pb displayed the highest strength compared with the specimens contaminated by Zn or Cr. Therefore, for specimens tested in the present work, the most notable detrimental effect on remediation efficacy was induced by $Cr^{3+}$, whereas the least was induced by $Pb^{2+}$; this is supported by Li et al. (2001), Olmo et al. (2001), and Kumpiene et al. (2008). In their reports, Qiao et al. (2007) and Chen et al. (2010) explained that $Pb^{2+}$ in solidified soils only hinders the hydration reaction of $C_3A$ and then reduces the quantity of the formed C-A-H. In contrast, for Zn-contaminated specimens, Olmo et al. (2001) reported that the $Zn(OH)_2$ precipitate formed on the solid particle surface isolates the cement from the pore water, and the replacement of $Ca^{2+}$ in the C-S-H gel by $Zn^{2+}$ forms an insoluble calcium silicate; both of these processes

**Fig. 4** Schematic diagram of electrical resistivity test

(a) Initial $Pb^{2+}$, $Zn^{2+}$, $Cr^{3+}$ concentrations of 0 mg/kg

(b) Initial $Pb^{2+}$ concentration of 10,000 mg/kg

(c) Initial $Zn^{2+}$ concentration of 10,000 mg/kg

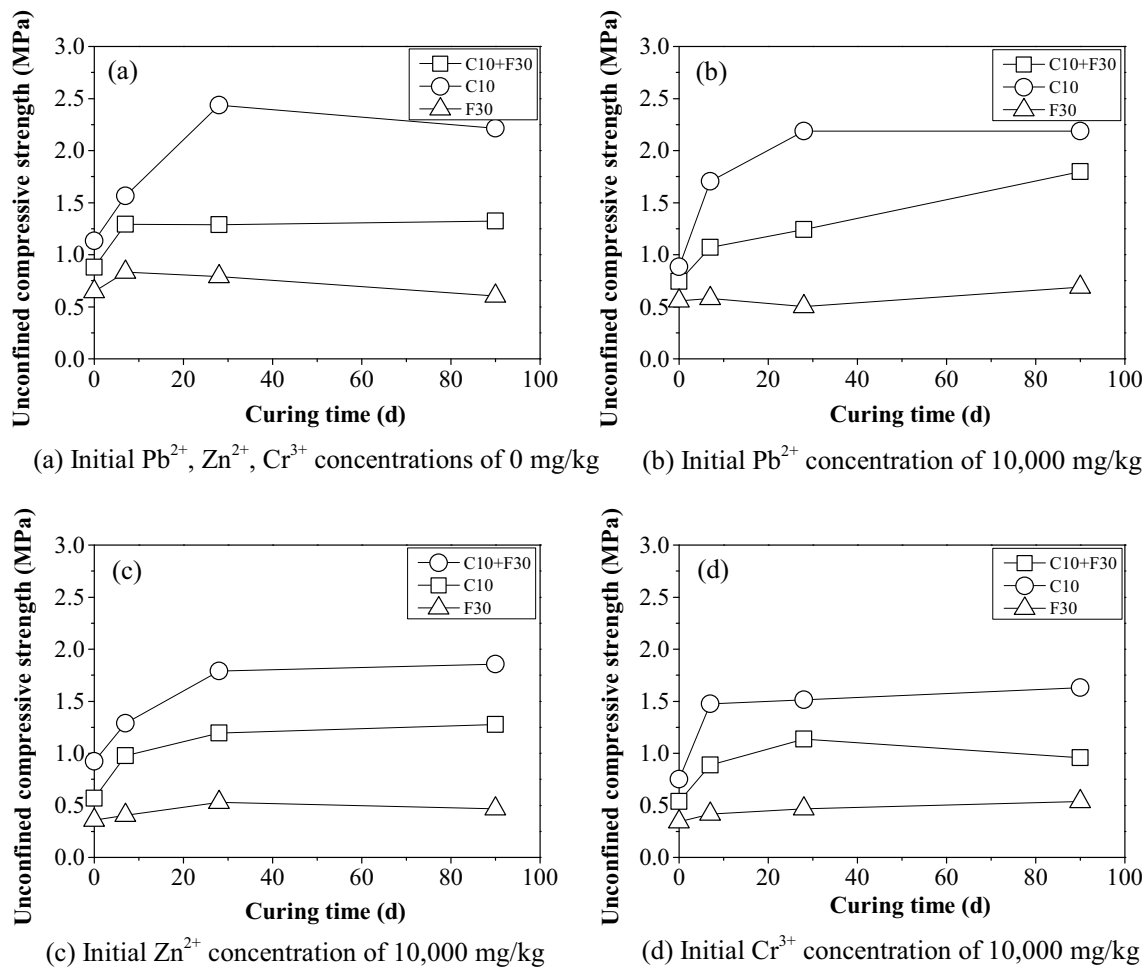(d) Initial $Cr^{3+}$ concentration of 10,000 mg/kg

Fig. 5 Unconfined compressive strength as a function of curing time

finally impede the hydration reaction and reduce the strength of the specimens. With respect to the Cr-contaminated specimens, Sophia et al. (2010) and Bhatty (1987) concluded that $Cr^{3+}$ could replace $Si^{4+}$, $Ca^{2+}$ in the C-S-H gel, supplant $Al^{3+}$ in the C-A-H gel, and displace $Al^{3+}$ in ettringite during the hydration reactions, ion exchanges and agglomerations, and pozzolanic reactions. Finally, the integrity of the solidified specimens initially contaminated by $Cr^{3+}$ was strongly affected, which resulted in the lowest strength compared with the specimens contaminated by $Pb^{2+}$ and $Zn^{2+}$.

## Leaching characteristic

The leached ion concentrations measured in the TCLP tests are plotted as a function of curing time in Fig. 7.

Results in Fig. 7 showed that the heavy metal ion concentrations in the leachate decreased rapidly in the initial period and stabilized as curing time increased further, which confirmed the remediation efficacy of cement/fly ash for the contaminated specimens. The

reason is that the hydration reactions, ion exchanges, and pozzolanic reactions of the cement/fly ash proceed with increasing curing time. The heavy metal ions are adsorbed onto the hydration gels and/or incorporated in the chemical formations by precipitation, substitution, or complexation (Li et al. 2001; Du et al. 2014; An et al. 2018; Wang et al. 2019). In addition, curves in Fig. 7 showed that the remediation efficacy of the cement/fly ash for the contaminated specimen was better than that of fly ash alone, which is consistent with the results presented in Fig. 5.

Results in Fig. 7 also showed that the initial concentration and type of heavy metal ion significantly influenced the leaching characteristics of the solidified specimens. Spence (1992) reported that $Pb^{2+}$ in the contaminated specimens was mainly solidified by adsorption onto hydrated gels, whereas $Zn^{2+}$ in the contaminated specimens could be precipitated in the alkaline environment created by cement/fly ash and encapsulated by or adsorbed onto the hydrated gels during the hydration process (Conner and Hoeffner 1998). When the

**Fig. 6** Relationships between unconfined compressive strength and initial ion concentration of specimens containing different heavy metal ions (C10+F30 additive; curing time of 90 days)
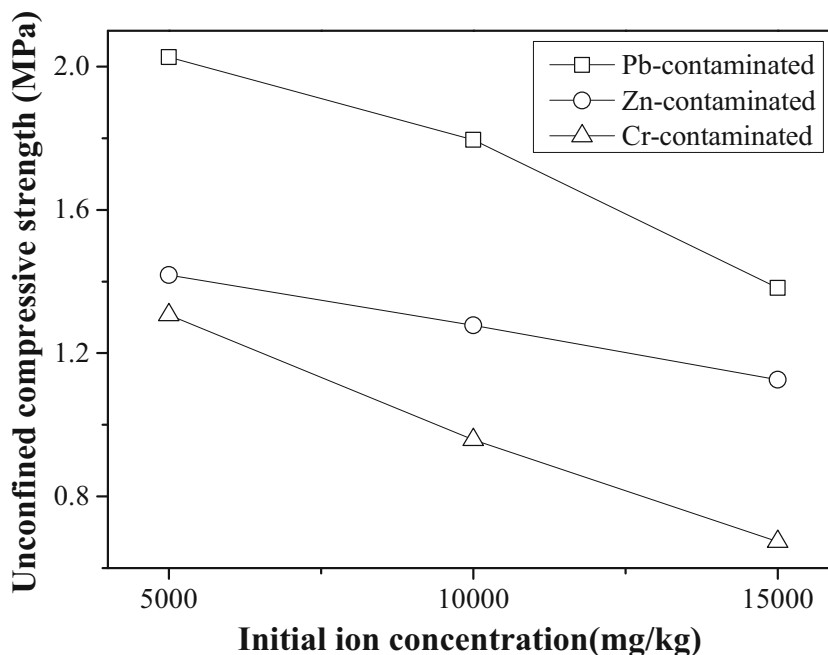
initial ion concentration increases to exceed the adsorption capacity, excessive $Pb^{2+}$ or $Zn^{2+}$ will be dissolved in the pore water and retard the hydrolysis and hydration processes, which reduces the stability of the solidification. However, compared to $Pb^{2+}$, the multiple solidification mechanisms of $Zn^{2+}$ implies less influence of acid leachate on the contaminated specimens, as presented in Fig. 8 (Tashiro et al. 1994). With respect to Cr-contaminated specimens, the encapsulation by and adsorption onto hydrated gels have notable effects on the solidification efficacy. Experiments performed by Pandey et al. (2012) also showed extremely low Cr concentrations in the leachate after TCLP tests.

## Electrical resistivity characteristic

The electrical resistivities as a function of curing time for the tested specimens are presented in Fig. 9.

As shown in Fig. 9, the electrical resistivity of tested specimen increased significantly with increasing curing



**Fig. 7** Leached ion concentration as a function of curing time (initial ion concentration of 10,000 mg/kg)
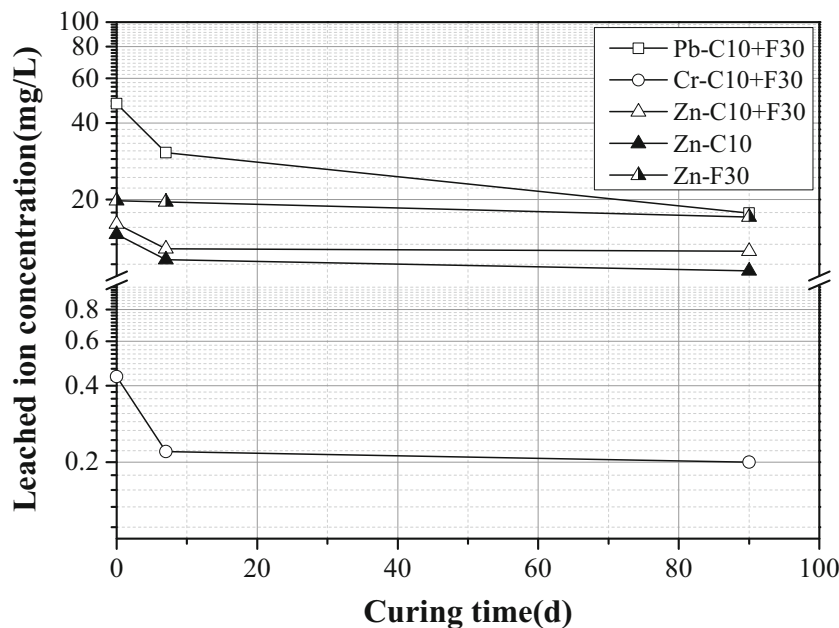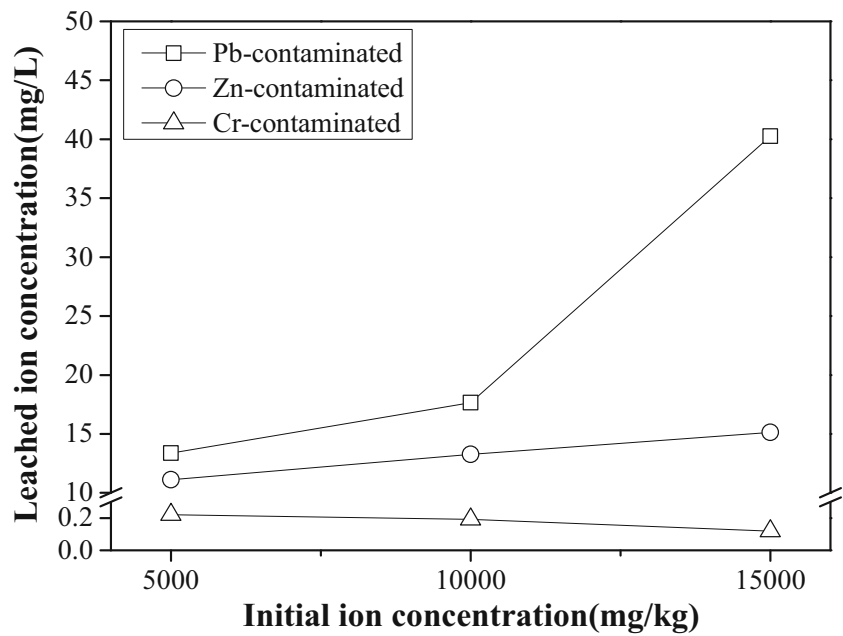
time. The electrical resistivity measured for the cement/fly ash–solidified specimen was lower and higher than that of the cement-solidified and the fly ash–solidified

specimens, respectively, which is consistent with the results presented in Figs. 5 and 7. Horpibulsuk et al. (2003) and Tang et al. (2018) reported similar results, and
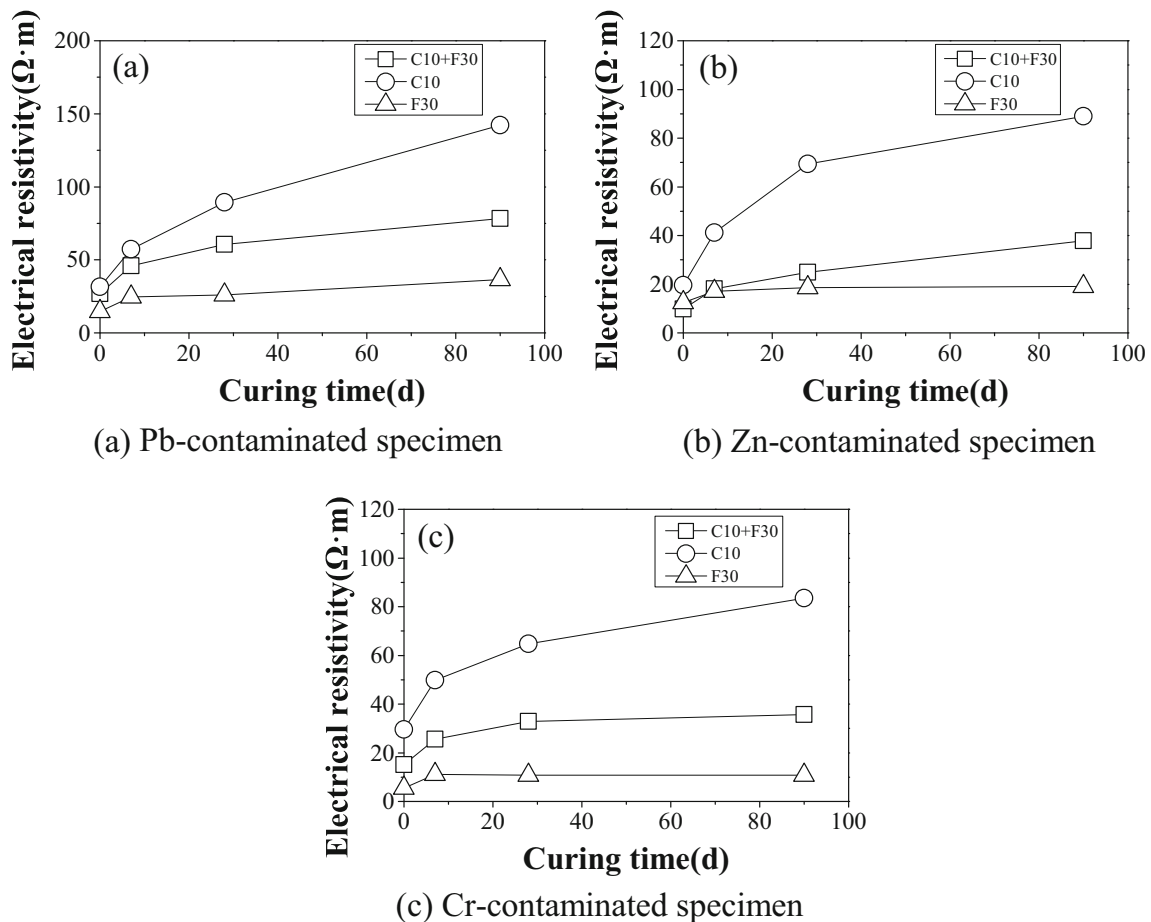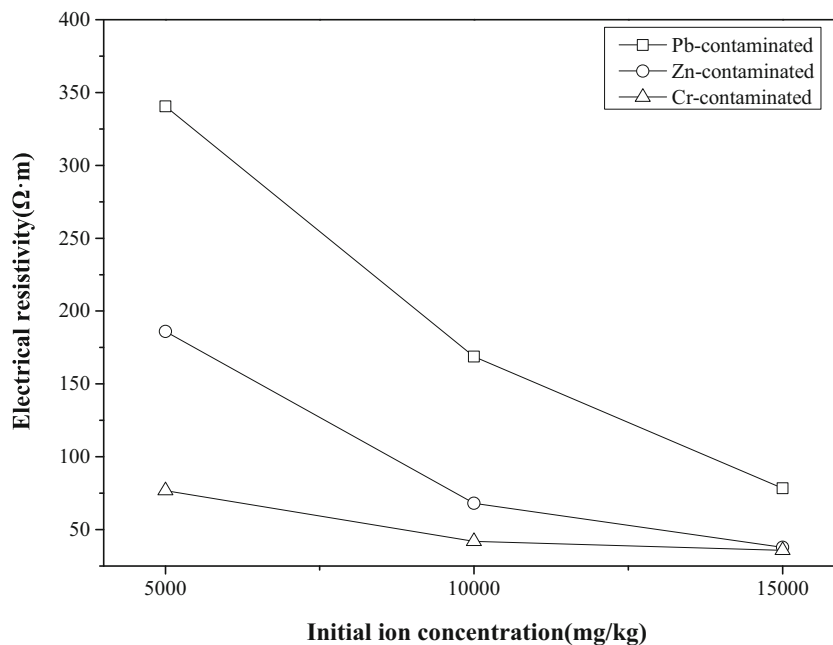


(a) Pb-contaminated specimen



(b) Zn-contaminated specimen



(c) Cr-contaminated specimen

**Fig. 9** Electrical resistivity as a function of curing time (initial ion concentration of 15,000 mg/kg)

explained that the pozzolanic reaction is enhanced during the curing stage leading to a decrease in water content of the specimen, and subsequently an increase in electrical resistivity. Complementing this, Bredenberg (2017) emphasized that the incorporation of fine particles into the hydration gels (such as C-S-H or C-A-H) resulted in a densified microstructure of the specimen, which increased the electrical resistivity owing to the lower electrical conductivity of soil particles than that of pore water.

The effects of initial concentration and type of heavy metal ions on the electrical resistivity of the solidified specimen are presented in Fig. 10.

As shown in Fig. 10, the electrical resistivity of the specimens decreased considerably with increasing initial ion concentration, and the evolution depended on the type of heavy metal in the specimen. According to studies performed by Kibria and Hossain (2012) and Oh et al. (2014), the addition of heavy metal ions and increase in concentration resulted in an increased cationic conductivity and decreased electrical resistivity of the specimen. Moreover, the higher heavy metal ion concentration retarded the hydration reaction and promoted a loose microstructure of the specimen, which then had a relatively low electrical resistivity (Boardman 1999). As described previously, the most notable detrimental effect on the hydration process was induced by $Cr^{3+}$, whereas the least was induced by $Pb^{2+}$ (Li et al. 2001; Olmo et al. 2001; Qiao et al. 2007; Kumpiene et al. 2008; Sophia et al. 2010). As a result, the electrical resistivity of the Pb-contaminated specimen was higher than that of the Zn-contaminated specimen, which in turn was higher than that of the Cr-contaminated specimen, as shown in Fig. 10.

## Prediction of strength and leaching characteristics using electrical resistivity

The strength and leaching characteristics are two key technical parameters for the assessment of remediation efficacy of the S/S technique. The efficacy could be predicted by the electrical resistivity measured in the present work owing to internal consistency in the microstructure characteristics.

Relationships between the unconfined compressive strength and the electrical resistivity for cement/ fly ash–solidified specimens with different initial ion concentrations are presented in Fig. 11.

Figure 11 clearly showed that the unconfined compressive strength increased with increasing electrical resistivity. Linear relationships on a semi-log scale consistently occurred for specimens with different initial ion concentrations. Therefore, Eq. (2) could be adopted to fit the results shown in Fig. 11 as follows:

$$q_u = a + b \cdot lg(\rho) \tag{2}$$

where $q_u$ (in MPa) and $\rho$ (in $\Omega \cdot m$) are the unconfined compressive strength and electrical resistivity of the tested specimen, respectively; and $a$ and $b$ are fitting parameters based on the test results.

Based on Fig. 11 and Eq. (2), the fitting parameters $a$ and $b$ and the coefficient of determination for different specimens are summarized in Table 3.
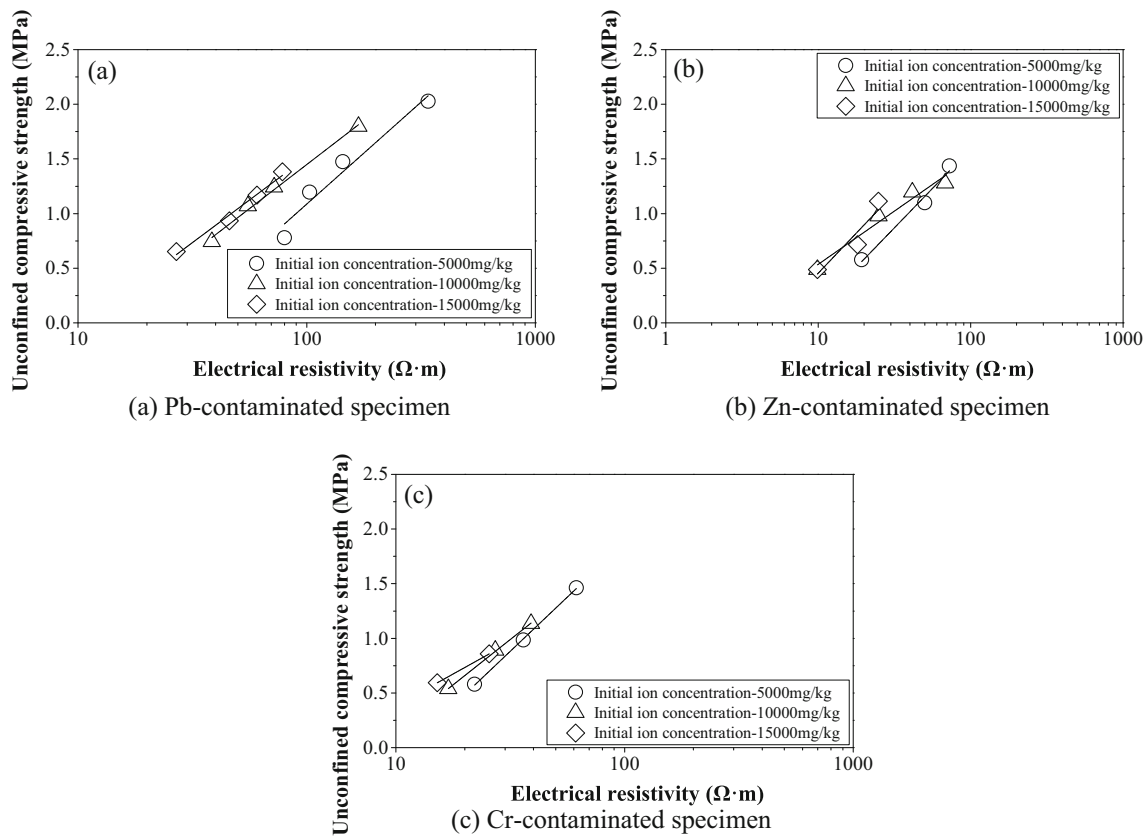
**Fig. 10** Relationships between electrical resistivity and initial ion concentration of specimens containing different heavy metal ions (C10+F30 additive; curing time of 28 days)

(a) Pb-contaminated specimen

(b) Zn-contaminated specimen

(c) Cr-contaminated specimen

**Fig. 11** Relationships between unconfined compressive strength and electrical resistivity of tested specimens

The extracted fitting parameters $a$ and $b$ are plotted as a function of the initial ion concentration in Fig. 12

Results in Fig. 12 showed that, for specimens contaminated by different heavy metal ions, changes in initial ion concentration did not result in notable variations in either $a$ or $b$, which confirmed the unique relationship between the unconfined compressive strength and the electrical resistivity. In this scenario, Eqs. (3–5) could be obtained by inserting the average values of the fitting parameters into Eq. (2).

Pb−contaminated soils $\qquad qu = -2.01 + 1.68 \cdot lg(\rho)$ (3)

Zn−contaminated soils $\qquad q_u = -0.91 + 1.29 \cdot lg(\rho)$ (4)

Cr−contaminated soils $\qquad q_u = -1.46 + 1.60 \cdot lg(\rho)$ (5)

Similarly, relationships between the leached ion concentration and the electrical resistivity for cement/fly ash–solidified specimens with different initial ion concentrations are presented in Fig. 13.

Results in Fig. 13 consistently showed that linear relationships on a semi-log scale could be adopted to describe the decreasing trend of the leached ion

concentration as a function of electrical resistivity, as shown in Eq. (6).

$$C_L = c + d \cdot lg(\rho) \qquad (6)$$

where $C_L$ (in mg/L) is the ion concentration in the leachate measured in the TCLP test; and $c$ and $d$ are fitting parameters. The fitting parameters and the coefficient of determination were determined based on Fig. 13 and Eq. (6), and are summarized in Table 4.

**Table 3** Fitting results in relationships between unconfined compressive strength and electrical resistivity

| Heavy metal | Initial ion concentration (mg/kg) | Fitting parameter | | Coefficient of determination |
|---|---|---|---|---|
| | | $a$ | $b$ | |
| Pb | 5,000 | − 2.65 | 1.87 | 0.937 |
| | 10,000 | − 1.77 | 1.61 | 0.991 |
| | 15,000 | − 1.61 | 1.56 | 0.975 |
| Zn | 5,000 | − 1.29 | 1.44 | 0.969 |
| | 10,000 | − 0.44 | 0.97 | 0.948 |
| | 15,000 | − 1.01 | 1.47 | 0.785 |
| Cr | 5,000 | − 2.10 | 1.99 | 0.984 |
| | 10,000 | − 1.50 | 1.66 | 0.978 |
| | 15,000 | − 0.78 | 1.16 | 0.979 |

**Fig. 12** Fitting parameters *a* and *b* for various initial ion concentrations in specimens
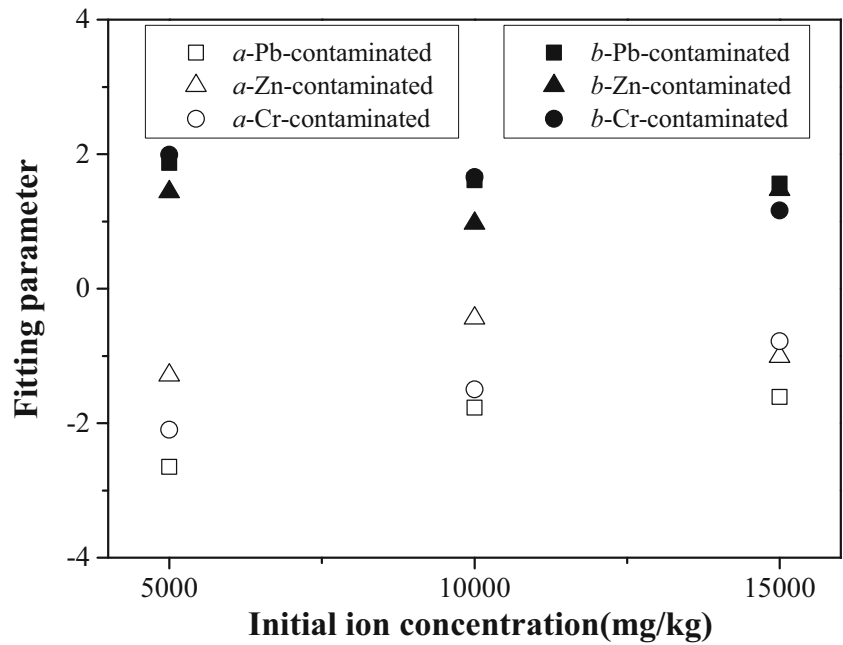
The fitting parameters *c* and *d* as a function of initial concentration of heavy metal ions in the specimens are presented in Fig. 14.

As shown in Fig. 14, the values of the fitting parameters remained almost constant for Zn- and Cr-contaminated specimens with different initial ion
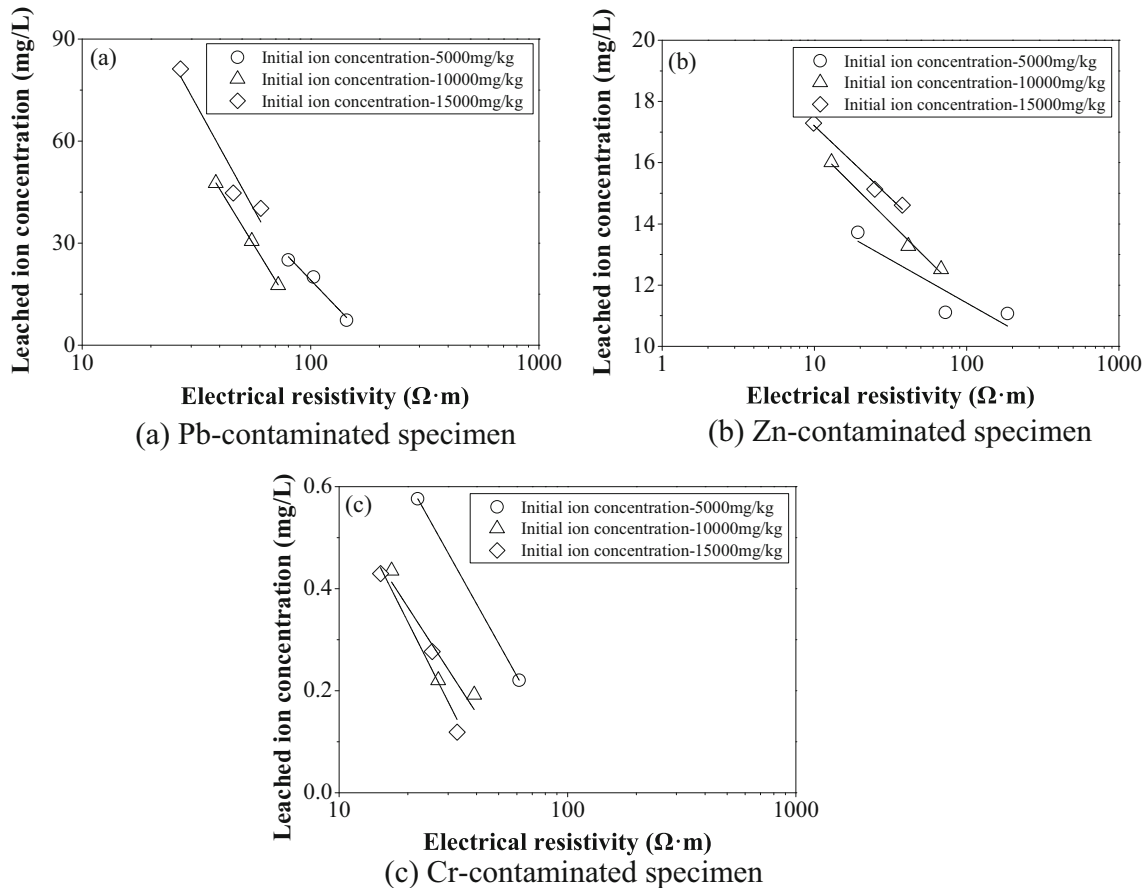


(a) Pb-contaminated specimen

(b) Zn-contaminated specimen

(c) Cr-contaminated specimen

**Fig. 13** Relationships between leached ion concentration and electrical resistivity of tested specimens

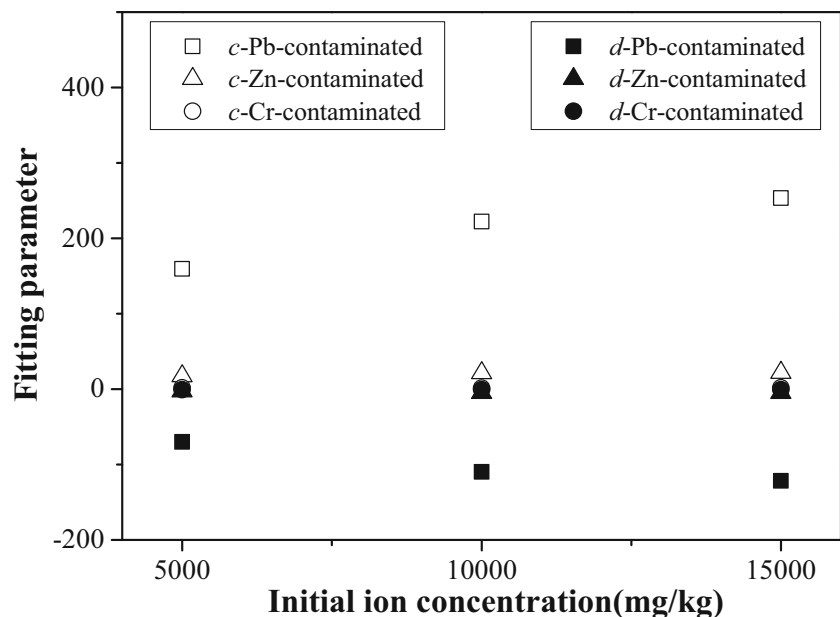**Table 4** Fitting results in relationships between leached ion concentration and electrical resistivity

| Heavy metal | Initial ion concentration (mg/kg) | Fitting parameter | | Coefficient of determination |
|---|---|---|---|---|
| | | $c$ | $d$ | |
| Pb | 5,000 | 159.48 | − 70.14 | 0.944 |
| | 10,000 | 221.96 | − 109.89 | 0.997 |
| | 15,000 | 253.31 | − 121.80 | 0.884 |
| Zn | 5,000 | 17.06 | − 2.82 | 0.674 |
| | 10,000 | 21.46 | − 4.95 | 0.984 |
| | 15,000 | 21.92 | − 4.72 | 0.967 |
| Cr | 5,000 | 1.65 | − 0.80 | 0.998 |
| | 10,000 | 1.26 | − 0.69 | 0.777 |
| | 15,000 | 1.49 | − 0.89 | 0.912 |

concentrations. Insignificant variations of the fitting parameters can be observed for specimens contaminated by Pb. Considering the wide range of initial ion concentrations adopted in the present work and the simplicity of the application, average values of the fitting parameters were determined and introduced into Eq. (6). As a result, the relationships between the leached ion concentration and the electrical resistivity of the specimens contaminated by different heavy metal ions could be presented in Eqs. (7-9).

Pb−contaminated soils $\qquad C_L = 221.58 - 100.61 \cdot lg(\rho)$ (7)

Zn−contaminated soils $\qquad C_L = 20.15 - 4.16 \cdot lg(\rho)$ (8)

Cr−contaminated soils $\qquad C_L = 1.47 - 0.79 \cdot lg(\rho)$ (9)

Based on Eqs. (3–5) and Eqs. (7-9), the key technical parameters, including the unconfined compressive strength and the leached ion concentration, can be determined and predicted once the corresponding electrical resistivity is measured. In this manner, the remediation efficacy of heavy metal–contaminated soils solidified by cement/fly ash can be assessed in a simple manner owing to the efficiency and cost-effectiveness of the electrical resistivity technique (Feng et al. 2017; Cao et al. 2018).

## Conclusions

In the present work, unconfined compressive strength and TCLP tests were performed to investigate the strength and leaching characteristics of heavy metal–contaminated soils solidified/stabilized by cement/fly ash. Electrical resistivity was also measured to establish empirical relationships for the assessment of remediation efficacy. Some main conclusions could be drawn as follows:

1. The unconfined compressive strength increased and the leached ion concentration decreased with increasing curing time, which confirmed the efficacy of cement/fly ash for remediation of heavy metal–contaminated soils.
2. The unconfined compressive strength decreased and the leached ion concentration increased with increasing initial heavy metal concentration in the specimen.
3. The type of heavy metal significantly influenced the strength and leaching characteristics of the specimens.



**Fig. 14** Fitting parameters $c$ and $d$ for various initial ion concentrations in specimens

For the strength characteristic, the most notable detrimental effect on remediation was induced by $Cr^{3+}$, whereas the least was induced by $Pb^{2+}$. For the leaching characteristic, the trend was reversed.

4. The electrical resistivity of the tested specimens increased significantly with increasing curing time and with decreasing concentration, which also depended on the types of heavy metal ions in the specimen. The electrical resistivity of the Pb-contaminated specimen was higher than that of the Zn-contaminated specimen, which in turn was higher than that of the Cr-contaminated specimen.

5. Linear relationships on a semi-log scale consistently occurred for changes in the unconfined compressive strength and leached ion concentration with the electrical resistivity. The fitting parameters were almost constant, providing a simple and fast method to assess the remediation efficacy of heavy metal–contaminated soils solidified/stabilized by cement/fly ash.

# References

An N, Tang CS, Xu SK, Gong XP, Shi B, Inyang HI (2018) Effects of soil characteristics on moisture evaporation. Eng Geol 239:126–135

ASTM D2166 / D2166M-16 (2016) Standard test method for unconfined compressive strength of cohesive soil. ASTM International, West Conshohocken

ASTM D2216-10 (2010) Standard test methods for laboratory determination of water (moisture) content of soil and rock by mass. ASTM International, West Conshohocken, PA, USA

ASTM D2487-00 (2000) Standard classification of soils for engineering purposes (Unified Soil Classification System). ASTM International, West Conshohocken, PA

ASTM D4318-17e1 (2017) Standard test methods for liquid limit, plastic limit, and plasticity index of soils. ASTM International, West Conshohocken, PA,USA

ASTM G187-05 (2005) Standard test method for measurement of soil resistivity using the two-electrode soil box method. ASTM International, West Conshohocken, PA

Bhatty, M. S. Y., 1987. Fixation of metallic ions in Portland cement. Proceedings of 4th National Conference on Hazardous Wastes and Hazardous Materials. 140–145.

Bian X, Cui YJ, Li XZ (2018) Voids effect on the swelling behaviour of compacted bentonite. Géotechnique. 69(7):593–605 1-13

Boardman, D. I., 1999. Lime stabilisation: clay-metal-lime interactions (PhD thesis) Loughborough University, Leicestershire.

Bredenberg, H., 2017. Dry mix methods for deep soil stabilization. Routledge.

Cao Z, Xiang L, Peng E, Li K (2018) Experimental study on electrical resistivity of cement-stabilized lead-contaminated soils. Adv Civ Eng 2018:11

Chen L, Liu SY, Du YJ (2010) Study on strength characteristics of cement-solidified heavy metal Pb-contaminated soils. Chin J Geotechn Eng 32(12):1898–1903 (in Chinese)

Chen QY, Hills CD, Tyrer M, Slipper I, Shen HG, Brough A (2007) Characterisation of products of tricalcium silicate hydration in the presence of heavy metals. J Hazard Mater 147(3):817–825

Chen YG, He Y, Ye WM, Jia LY (2015) Competitive adsorption characteristics of Na (I)/Cr (III) and Cu (II)/Cr (III) on GMZ bentonite in their binary solution. J Ind Eng Chem 26:335–339

Chen ZG, Tang CS, Zhu C, Shi B, Liu YM (2017) Compression, swelling and rebound behavior of GMZ bentonite/additive mixture under coupled hydro-mechanical condition. Eng Geol 221:50–60

Conner JR, Hoeffner SL (1998) A critical review of stabilization/solidification technology. CRC Crit Rev Environ Control 28(4):397–462

Deng YF, Yue X, Liu S, Chen Y, Zhang D (2015) Hydraulic conductivity of cement-stabilized marine clay with metakaolin and its correlation with pore size distribution. Eng Geol 193:146–152

Deng Y, Liu Q, Cui Y, Wang Q, Liu S (2018) Revisiting relationships among specific surface area, soil consistency limits, and group index of clays. J Test Eval 47:1392–1404

Du YJ, Wei ML, Reddy KR, Liu ZP, Jin F (2014) Effect of acid rain pH on leaching behavior of cement stabilized lead-contaminated soil. J Hazard Mater 271:131–140

Feng SJ, Bai ZB, Cao BY, Lu SF, Ai SG (2017) The use of electrical resistivity tomography and borehole to characterize leachate distribution in Laogang landfill, China. Environ Sci Pollut R 24(25):20811–20817

Horpibulsuk S, Miura N, Nagaraj TS (2003) Assessment of strength development in cement-admixed high water content clays with Abrams' law as a basis. Geotechnique. 53(4):439–444

Hunce SY, Akgul D, Demir G, Mertoglu B (2012) Solidification/stabilization of landfill leachate concentrate using different aggregate materials. Waste Manag 32(7):1394–1400

Katsioti M, Katsiotis N, Rouni G, Bakirtzis D, Loizidou M (2008) The effect of bentonite/cement mortar for the stabilization/solidification of sewage sludge containing heavy metals. Cement and Concrete Comp 30(10):1013–1019

Kibria G, Hossain MS (2012) Investigation of geotechnical parameters affecting electrical resistivity of compacted clays. J Geotech Geoenviron 138(12):1520–1529

Kolias S, Kasselouri-Rigopoulou V, Karahalios A (2005) Stabilisation of clayey soils with high calcium fly ash and cement. Cement and Concrete Comp 27(2):301–313

Kumpiene J, Lagerkvist A, Maurice C (2008) Stabilization of As, Cr, Cu, Pb and Zn in soil using amendments–a review. Waste Manag 28(1):215–225

Levasseur B, Chartier M, Blais JF, Mercier G (2006) Metals removal from municipal waste incinerator fly ashes and reuse of treated leachates. J Environ Eng 132(5):497–505

Li JS, Wang L, Cui JL, Poon CS, Beiyuan J, Tsang DCW, Li XD (2018) Effects of low-alkalinity binders on stabilization/solidification of geogenic As-containing soils: spectroscopic investigation and leaching tests. SciTotal Environ 631-632:1486–1149

Li XD, Poon CS, Sun H, Lo IMC, Kirk DW (2001) Heavy metal speciation and leaching behaviors in cement based solidified/stabilized waste materials. J. Hazard Mater 82(3):215–230

Liu LW, Li W, Song WP, Guo MX (2018) Remediation techniques for heavy metal-contaminated soils: Principles and applicability. Sci Total Environ 633:206–219

Liu L, Zhou A, Deng Y, Cui Y, Yu Z, Yu C (2019) Strength performance of cement/slag-based stabilized soft clays. Constr Build Mater 211:909–918

Miller J, Akhter H, Cartledge FK, Mclearn M (2000) Treatment of arsenic-contaminated soils. II: Treatability study and remediation. J Environ Eng 126(11):1004–1012

Moon DH, Grubb DG, Reilly TL (2009) Stabilization/solidification of selenium-impacted soils using Portland cement and cement kiln dust. J Hazard Mater 168(2):944–951

Nochaiya T, Wongkeo W, Chaipanich A (2010) Utilization of fly ash with silica fume and properties of Portland cement–fly ash–silica fume concrete. Fuel. 89(3):768–774

Oh TM, Cho GC, Lee C (2014) Effect of soil mineralogy and pore-water chemistry on the electrical resistivity of saturated soils. J Geotech Geoenviron 140(11):06014012

Olmo IF, Chacon E, Irabien A (2001) Influence of lead, zinc, iron (III) and chromium (III) oxides on the setting time and strength development of Portland cement. Cem Concr Res 31(8):1213–1219

Pandey B, Kinrade SD, Catalan LJJ (2012) Effects of carbonation on the leachability and compressive strength of cement-solidified and geopolymer-solidified synthetic metal wastes. J Environ Manag 101(2):59–67

Penilla RP, Bustos AG, Elizalde SG (2006) Immobilization of Cs, Cd, Pb and Cr by synthetic zeolites from Spanish low-calcium coal fly ash. Fuel. 85(5-6):823–832

Qiao XC, Poon CS, Cheeseman CR (2007) Investigation into the stabilization/solidification performance of Portland cement through cement clinker phases. J Hazard Mater 139(2):238–243

Sophia CA, Sandhya S, Swaminathan K (2010) Solidification and stabilization of chromium laden wastes in cementitious binders. Curr Sci India 99(3):365–369

Spence, R. D., 1992. Chemistry and microstructure of solidified waste forms. CRC Press.

Suman Raj DS, Aparna C, Rekha P, Bindhu VH, Anjaneyulu Y (2005) Stabilization and solidification technologies for the remediation of contaminated soils and sediments - an overview. Land Con Reclam 13(1):23–48

Tang CS, Shi B, Zhao LZ (2010) Interfacial shear strength of fiber reinforced soil. Geotext Geomembr 28(1):54–62

Tang CS, Wang DY, Zhu C, Zhou QY, Xu SK, Shi B (2018) Characterizing drying-induced clayey soil desiccation cracking process using electrical resistivity method. Appl Clay Sci 152:101–112

Tashiro C, Ikeda K, Inoue Y (1994) Evaluation of pozzolanic activity by the electric resistance measurement method. Cem Concr Res 24(6):1133–1139

USEPA, Method 1311, (1992). Toxicity characteristic leaching procedure//Office of Solid Waste and Emergency Response (Ed.). Test Methods for Evaluating Solid Waste. SW-846, U.S. Environmental Protection Agency, Washington.

Vipulanandan C (1995) Effect of clays and cement on the solidification/stabilization of phenol-contaminated soils. Waste Manag 15(5/6):399–406

Wang LL, Tang CS, Shi B, Cui YJ, Zhang GQ, Hilary I (2018) Nucleation and propagation mechanisms of soil desiccation cracks. Eng Geol 238:27–35

Wu Z, Deng Y, Cui Y, Zhou A, Feng Q, Xue H (2018) Experimental study on creep behavior in oedometer tests of reconstituted soft clays. Int J Geomech 19(3):04018198

Wang Y, Wang HS, Tang CS, Gu K, Shi B, 2019. Remediation of heavy metal contaminated soils by biochar: a review. Environ. Geotech. 1-14.

Yin CY, Mahmud HB, Shaaban MG (2006) Stabilization/solidification of lead-contaminated soil using cement and rice husk ash. J Hazard Mater 137(3):1758–1764

Yoon G, Oh M, Park J (2002) Laboratory study of landfill leachate effect on resistivity in unsaturated soil using cone penetrometer. Environ Geol 43(1-2):18–28

Zha F, Liu J, Deng Y, Xu L, Wang X, Yang X (2018, October) Solidification/Stabilization (S/S) of high concentration zinc-contaminated soils using soda residue. In: The International Congress on Environmental Geotechnics. Springer, Singapore, pp 683–690

Zha FS, Xu L, Cui KR (2012) Study on strength characteristics of heavy metal contaminated soils solidified/stabilized by cement. Rock Soil Mech 33(3):652–656 (in Chinese)

Zhang D, Cao Z, Fan L, Liu S, Liu W (2014) Evaluation of the influence of salt concentration on cement stabilized clay by electrical resistivity measurement method. Eng Geol 170:80–88